

COMMISSIONING OF THE X-BAND TRANSVERSE DEFLECTOR FOR FEMTOSECOND ELECTRON/X-RAY PULSE LENGTH MEASUREMENTS AT LCLS

Y. Ding, C. Behrens, J. Frisch, Z. Huang, P. Krejcik, J. Lewandowski, H. Loos, J. Wang, M-H. Wang, J. Welch
 SLAC National Accelerator Laboratory, Menlo Park, CA 94025, USA

Abstract

X-ray free-electron lasers provide ultrashort x-ray pulses from several to a few hundred femtoseconds for multidisciplinary users. However, tremendous challenges remain in the measurement and control of these ultrashort pulses with femtosecond precision, for both the electron bunch and the x-ray pulse. A new diagnostic scheme adding a transverse radio-frequency deflector at the end of the linac coherent light source (LCLS) undulator beamline has been proposed earlier. Two 1-m long deflecting structures have been installed at LCLS during the summer of 2012. Installation of the high power RF components including the klystron, waveguide, RF controls etc. has finished and commissioning has started since the spring of 2013. We report the latest progress of the commissioning of the deflector at LCLS.

INTRODUCTION

Generation and characterization of ultrashort electron and x-ray beams are interesting and challenging topics in x-ray free-electron lasers (FEL). At the Linac Coherent Light Source (LCLS), since its first operation in 2009 [1], two additional operation modes – low charge and slotted-foil – have been developed for generation of x-ray pulses less than 10 fs [2, 3, 4]. Temporal diagnostics with femtosecond (fs) resolution has been also studied recently [5, 6].

Using a transverse rf deflector in conjunction with an e-beam energy spectrometer to characterize both the electron and x-ray pulse temporal profile was proposed in [7]. The beam is deflected horizontally with an rf deflector, and bent vertically with a spectrometer, hence the e-beam longitudinal phase space can be measured. This diagnostic system is located at the end of the LCLS undulator beamline. It provides a simple, single shot temporal diagnostic method that is non-invasive to the FEL operation. This project was funded in 2011 at LCLS. A status report can be found in [8]. In this paper we report the recent status of the project and the initial commissioning progress.

DESIGN AND SIMULATIONS

In the FEL process, the interaction between an e-beam and an electromagnetic wave causes electron energy loss and energy spread increase. For example, at LCLS, the typical FEL-induced electron energy loss at saturation is more than 10 MeV [1]. By measuring the electron longitudinal phase space at FEL-on and FEL-off condition, we can retrieve the time-resolved electron beam energy loss or

energy spread increase due to FEL lasing process. In this way the x-ray temporal profile can be obtained if the slippage effect is small. Figure 1 shows the beamline layout of this diagnostic system being installed at the end of the LCLS undulator. We use two 1-meter long X-band rf deflecting structures in this design. The structure rf frequency is 11.424 GHz, working at a $2\pi/3$ backward-wave TM11 mode. An X-band rf deflector has been chosen over an S-band one in order to impart a stronger sweep to the beam and thus improve the temporal resolution. The maximum horizontal kick of the design is 48 MeV/c, with 40 MW input rf power at the deflecting structure [9].

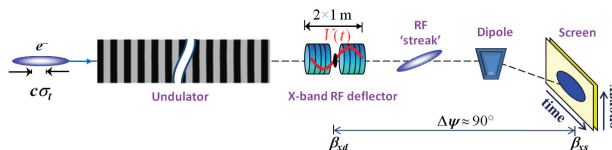


Figure 1: A layout of the diagnostic system with a transverse rf deflector and an energy spectrometer.

Start-to-end simulations have been carried out to verify this scheme. Here we show an example of the LCLS hard x-ray case (radiation wavelength of 1.5 Å, e-beam energy of 13.6 GeV, total undulator length of 132m including breaks) with a charge of 250 pC [7]. The average e-beam peak current is set at about 3 kA. Figures 2(a) and 2(b) show the simulated “measurements” of the projected transverse images at the dump screen, with the horizontal axis representing time, and the vertical axis representing energy. Clearly, we can see the difference in the energy dimension between FEL-on and FEL-off. From the two images we can determine the time-sliced energy loss or energy spread increase purely induced from the FEL radiation.

The horizontal projection of the images in Fig. 2(a) and 2(b) represents the e-beam temporal profile $I(t)$. With the obtained time-sliced energy loss and current, the x-ray power profile is directly determined with an absolute power scale ($P(t) = \Delta E_{FEL}(t)/e \times I(t)$). The reconstructed x-ray profile from the energy loss for this hard x-ray example is shown in Fig. 2(d). Since LCLS is operating in the self-amplified spontaneous emission (SASE) mode, there are many longitudinal spikes whose typical width is ~ 0.2 fs in this wavelength. The reconstructed pulse shape is a smooth approximation to the actual profile, where the finer spikes are smeared out due to the limited temporal resolution.

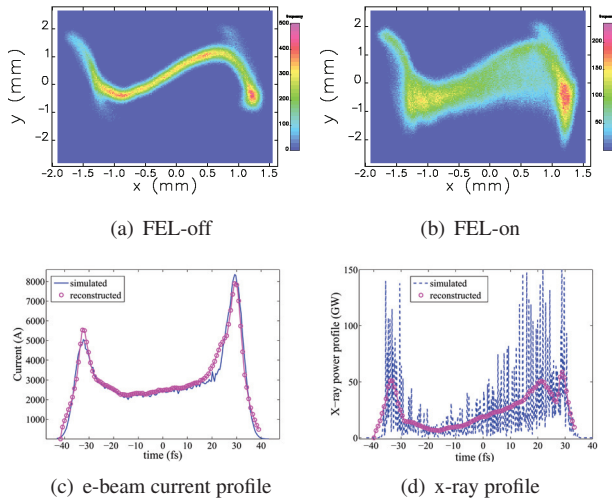


Figure 2: The simulated images on the screen representing e-beam longitudinal phase space for FEL-off (a) and FEL-on (b). (c) and (d) show the reconstructed e-beam current and FEL x-ray profiles (magenta) comparing with the simulated ones (blue). Bunch head is to the left [7].

OPTICS OPTIMIZATION AND COMMISSIONING

In this design, the electron beam is deflected horizontally, and we can define a temporal calibration factor as

$$S = \frac{\sigma_x}{c\sigma_t} = \frac{eV_0}{pc} \sqrt{\beta_{xd}\beta_{xs}} |\sin\Delta\Psi| \frac{2\pi}{\lambda}. \quad (1)$$

Here V_0 is the deflecting voltage, β_{xd} and β_{xs} are horizontal beta functions at the deflector and the screen. $\Delta\Psi$ is the phase advance between the deflector and the screen, and $\lambda = 2.63\text{cm}$ for a frequency of 11.424 GHz. Temporal resolution $\sigma_{t,r}$ can be written as

$$\sigma_{t,r} = \frac{\sqrt{\sigma_{x0}^2 + \sigma_{screen}^2}}{cS} \propto \sqrt{\frac{\epsilon_n}{\gamma\beta_{xd}} + \frac{\sigma_{screen}^2}{\beta_{xd}\beta_{xs}}} \quad (2)$$

Here σ_{x0} is the nominal horizontal beam size at the screen (i.e., without deflecting). Note that we include the term due to screen and/or camera resolution σ_{screen} . Without considering screen resolution, we only have the first term in Eq. (3), which gives a theoretical resolution, and a larger horizontal beta function at the deflector location is preferred. Once including the screen/camera resolution, we also hope to have a larger beta function β_{xs} on the screen.

The vertical beam size measured after the vertically-bent spectrometer represents the electron energy deviation, and the energy resolution $\sigma_{E,r}$ can be defined as

$$\sigma_{E,r} = \frac{E_0}{\eta_{ys}} \sqrt{\frac{\beta_{ys}\epsilon_n}{\gamma} + \sigma_{screen}^2}, \quad (3)$$

where η_{ys} is the vertical momentum dispersion function at the screen, β_{ys} is vertical beta function at the screen, and

E_0 is the average electron energy. In the vertical dimension, a larger dispersion and smaller beta function at the screen are preferred.

To reserve space for future applications right after the LCLS undulator, we put the deflector at the very end of the beamline just before the bending magnets. One quadrupole magnet has been relocated in the beamline for achieving a better resolution. The optimized optics results and calculated resolutions are summarized in Table 1. Note the quad strength in the undulator region are fixed at different energies. A transverse matching section before the undulator is used to match beams into the undulator. As a result, the twiss parameters out of the undulator vary at different beam energies. These set different initial optics conditions for the deflector, and we have to adjust dump optics for the best deflector operation when energy changes. In this table, the screen/camera resolution here is assumed $30\ \mu\text{m}$ rms (from $50\ \mu\text{m}$ thickness YAG screen). A possibility of using OTR with an aluminum foil is under discussion, which can help further improve the resolution.

Table 1: X-band transverse deflector parameters.

Energy (GeV)	4.3	9.6	13.6
rf input power (MW)	40	40	40
Deflecting voltage (MV)*	48	48	48
Deflector horizon. β_{xd} (m)	372	148	111
Screen horizon. β_{xs} (m)	7.0	16.8	22.6
Screen vertical β_{ys} (m)	1.3	1.5	1.4
Screen vert. disper. η_{ys} (m)	0.52	0.59	0.6
Phase advance $\Delta\Psi$ (deg)	90	90	90
Emittance ϵ_n (μm)	1	1	1
betatron beam size σ_{x0} (μm)	28.8	29.9	29.1
betatron beam size σ_{y0} (μm)	12.4	8.8	7.4
Calibration factor S	136	60	42
Theor. temporal resol. (fs)	0.7	1.7	2.3
Temporal resol. w. screen (fs) \diamond	1.0	2.4	3.3
Theor. energy resol. (keV)	103	144	168
Energy resol. w. screen (keV) \diamond	270	511	704

* :The maximum kick for each structure (20MW each):

$$kick[MV] = 5.46\sqrt{P_{in}[MW]}.$$

\diamond : assuming screen resol. = $30\ \mu\text{m}$.

We tested the optics with an orbit response method. The beam was kicked using a corrector before the deflector, then we measured the beam centroid position from BPMs and compare them with the model predictions. Figure 3 shows an example of the measured orbit response while kicking the beam horizontally using XCUE1, located before the deflector. We got a reasonable agreement. To suppress the FEL lasing for baseline measurement, a local oscillation bump has been made, where we horizontally kick the beam using the first corrector in the beginning of the undulator, and kick the beam back using the last two correctors at the end of the undulator. In this way, the orbit out of the undulator comes back flat while the lasing is suppressed.

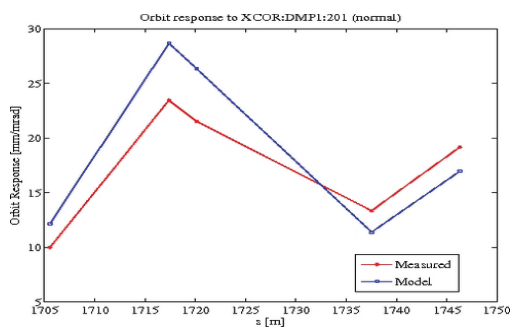


Figure 3: The orbit response between measurement and model prediction.

HARDWARE AND SOFTWARE COMMISSIONING

Two adjacent 1-m long X-band deflecting structures were installed at the end of the undulator beamline during 2012 summer [8]. After that, we have been continuing working on this project to add the waveguide, klystron and modulator, low-level rf system, control and protection systems, and other supporting devices. The whole system is ready to start high power rf processing and conditioning at the beginning of May 2013. After rf conditioning, low-level rf system will be calibrated and rf control software will be further tested. We expect to start beam-based commissioning in the middle of May.

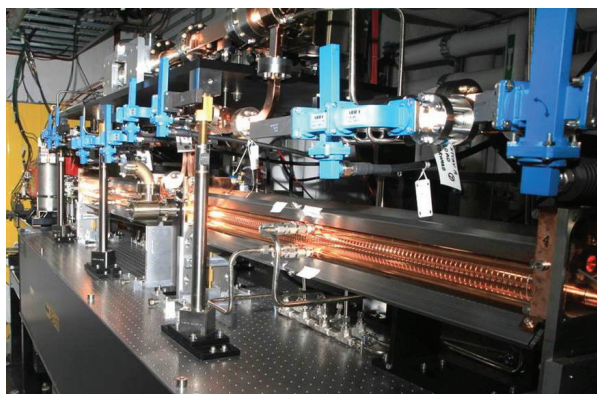


Figure 4: A photo of the deflector system installed at the undulator beamline. (Credit: P. Krejcik)

We show a photo of the installed structures in Fig. 4. The deflecting structures are fed by a single SLAC XL4 klystron housed together with a modulator in a support building above the undulator tunnel. RF waveguide mode converters are used to switch between WR90 rectangular waveguide and a low-loss over-moded WC293 circular waveguide at the klystron side and at the splitter to the two structures. The XL4 klystron delivers 50MW peak power at 120Hz and about 40 MW is delivered at the structure input couplers, based on recent measurements.

The relative phase and transverse alignment between the two structures are important for the resolution. The trans-

verse alignment was measured using the beam induced rf signals. We steered the electron beam horizontal orbit in the deflector area, recorded the BPM readings, and at the same time measured the excited rf signal at the waveguide port near the klystron using a peak power meter. In this way, the beam excites ~ 11.4 GHz HEM dipole mode and travels through backward wave “band pass filter” to the load. A clear rf signal intensity dip was observed when the BPM indicates the beam was on the center. The result shows the mechanical alignment is about $100 \mu\text{m}$ accuracy which is consistent with the initial design requirement.

The rf amplitude and phase jitters, together with the beam jitters due to energy, current and arrival time, have to be carefully dealt with. During the beam-based calibration, the rf phase readings from PAD and the beam arrival time measured from two phase cavities [10] will be used for jitter correction. In the case of a larger jitter, it might be even possible to get calibration factor by just sorting the jitter data (without changing the rf phase). During image processing, since we have to compare the lasing-off and lasing-on cases, the jitter correction is also critical for x-ray profile reconstruction. For lasing-off baseline data, we record multishot images, and apply the energy and current jitter correction to get sliced beam energy and energy spread, then average the slices from different shots to have a baseline sliced beam parameter. After switching on the FEL, we apply the same jitter corrections and slice analysis, then subtract the measured baseline background for each lasing shot. Matlab-based GUI have been developed to do this data analysis.

In summary, good progress has been made in the past two years for installation of the x-band transverse deflector at the LCLS undulator beamline. Commissioning of the whole system has just started in the spring of 2013. Once this diagnostic system is ready, it will provide single-shot based x-ray pulse diagnostics for the user experiments.

We thank SLAC engineering, controls, operations, safety, and rf support groups for their help and dedicated support. This work was supported by Department of Energy Contract No. DE-AC02-76SF00515.

REFERENCES

- [1] P. Emma et al., Nat. Photon. 4, 641 (2010).
- [2] Y. Ding et al., Phys. Rev. Lett. 102, 254801 (2009).
- [3] P. Emma et al., Phys. Rev Letter. 92, 074801 (2004).
- [4] Y. Ding et al., Phys. Rev Letter. 109, 254802 (2012).
- [5] H. Loos, SPIE conference, Proc. 8778-18, Czech Republic (2013);
- [6] Y. Ding et al., this IPAC13 proceedings, TUPEA086.
- [7] Y. Ding et al., Phys. Rev. ST AB 14, 120701 (2011);
- [8] P. Krejcik et al., THPB01 in IBIC12, Japan (2012).
- [9] J. Wang and S. Tantawi, in Proceedings of LINAC 08, Victoria, BC, Canada.
- [10] A. Brachmann et al., IPAC10; see also SLAC-PUB-14234.